





## Research Paper

## Application of Cellulose and Paper-Based Products in Building Acoustics

Aleksandra KLIMEK<sup>(1)\*</sup> , Jerzy F. ŁĄTKA<sup>(2)</sup> ,  
Paweł NIERADKA<sup>(1),(3)</sup> , Andrzej DOBRUCKI<sup>(1)</sup> 

<sup>(1)</sup> *Department of Acoustics, Multimedia and Signal Processing  
Wrocław University of Science and Technology  
Wrocław, Poland*

<sup>(2)</sup> *Department of Architecture and Visual Arts  
Wrocław University of Science and Technology  
Wrocław, Poland*

<sup>(3)</sup> *KFB Acoustics  
Wrocław, Poland*

\*Corresponding Author e-mail: [Aleksandra.Klimek@pwr.edu.pl](mailto:Aleksandra.Klimek@pwr.edu.pl)

(received July 5, 2023; accepted January 19, 2024; published online April 11, 2024)

This article presents a comprehensive acoustic study of paper-based building products: cellulose wool, paperboard, corrugated cardboard, and honeycomb panels. The material configurations included the intact form as well as the various modifications, i.e., density variation, multiple-layered staking, perforation or acoustic metamaterial setup. Tests covered acoustic absorption and insulation properties, with the last examined under excitation of both a plane wave and a diffused field. Additionally, the cellulose wool is provided with the characteristic impedance and propagation wavenumber results; and the paperboard was tested for its dynamic elastic and damping properties. The paper-based products, giving their weight, prove to be a convincing replacement for conventional materials by both absorptive and insulation performance. The maximum acquired sound reduction index, for exceptionally lightweight ( $2.2 \text{ kg/m}^2$ ) paper double-wall metamaterial structure, reached 26 dB.

**Keywords:** paper; cardboard; insulation; absorption; acoustic metamaterial; honeycomb.



Copyright © 2024 The Author(s).  
This work is licensed under the Creative Commons Attribution 4.0 International CC BY 4.0  
(<https://creativecommons.org/licenses/by/4.0/>).

## Acronyms

$C$ ,  $C_{tr}$  – sound reduction index correction factors,  
 $C_1$  – coefficient for 1st beam mode,  
 $E$  – Young’s modulus,  
 $H$  – spacing between the double walls,  
 $H_b$  – beam height in the vibration direction,  
 $H_R$  – height of the Helmholtz resonator,  
 $K$  – bulk modulus of air,  
 $K_{\text{eff}}$  – effective bulk modulus,  
 $S_R$  – cross section surface of the Helmholtz resonator neck,  
SRI – sound reduction index,  
TL – transmission loss,  
 $\mathcal{X}_{1,2}$  – angle related normalized wall impedance,  
 $X_{1,2}$  – normalized wall impedance,  
 $V_R$  – cavity volume of the Helmholtz resonator,

$\mathcal{Z}$  – angle related effective impedance,  
 $Z_{\text{eff}}$  – effective impedance,  
 $c$  – speed of sound in air,  
 $d_1$  – absorbent layer thickness,  
 $d_R$  – diameter of the Helmholtz resonator neck,  
 $f\omega$  – frequency, pulsation of wave,  
 $f_{01,2}$  – resonance frequency of double wall with the Helmholtz resonators system,  
 $f_{\text{DW}}$  – resonance frequency of a double wall,  
 $f_R$  – resonance frequency of the Helmholtz resonator,  
 $\Delta f$  – half-power bandwidth,  
 $k$  – wavenumber,  
 $k'$  – complex propagation wavenumber,  
 $k_{\text{eff}}$  – effective wavenumber,  
 $l$  – beam length,  
 $l_R$  – length of the Helmholtz resonator neck,  
 $m''_{1,2}$  – surface masses of double walls,

$z_1$  – rigid back absorbent surface impedance,  
 $z_c$  – complex characteristic impedance,  
 $\alpha$  – sound absorption coefficient,  
 $\zeta_R$  – the Helmholtz resonator damping ratio,  
 $\eta$  – damping loss factor,  
 $\theta, \psi$  – incident angle of acoustic wave,  
 $\theta_{\text{eff}}$  – angle of refraction,  
 $\tau$  – transmission coefficient,  
 $\phi_R$  – volumetric fill ratio of Helmholtz resonators,  
 $\rho$  – volumetric density,  
 $\rho_{\text{eff}}$  – effective density.

## 1. Introduction

Building industry is widely known as one of the most environmentally hazardous. It is responsible for 40 %–50 % of world greenhouse gas emissions (ABD RASHID, YUSOFF, 2015), 24 % material extraction from the lithosphere (ZABALZA BRIBIÁN *et al.*, 2011) and 40 % of global energy consumption (WANG *et al.*, 2023). Therefore, the research concerning building industry in the last decades emphasised new materials that minimise the environmental impact. On the other hand, more and more architectural structures and infill (such as interior partitions) are built for the limited period of time. After their life span, they should be recycled, upcycled or utilised in a way that reduces the environmental impact.

In the search of environmentally friendly and bio-based building materials, paper among materials such as wood, clay, adobe bricks, hempcrete, recycled plastics and glass, certified timber seems promising and fulfilling the building code requirements.

Paper is a material of natural origin, of which the main building component is cellulose, the most common natural polymer in the world. Its resources are considered inexhaustible (KLEMM *et al.*, 2005). Paper as a material formed by the network of cellulose fibres, which create a hydrogen bonds between each other, may be given different forms and characteristics. For building application, whether it is a structural element or partition, the following paper-based products are mostly often implemented (LATKA, 2017a; DIARTE, SHAFFER, 2021):

- paper tubes as linear and structural elements. Those products were vastly examined by Japanese architect Shigeru Ban, who implemented them in both temporary and permanent structures (MIYAKE *et al.*, 2009);
- cardboard profiles (*U*- and *L*-shapes), similarly like paper tubes are suitable as structural rod elements (LATKA, 2017b);
- corrugated cardboard, the most popular product used in packaging, which can serve as planar elements, i.e., wall, floor and roof panels. This product, due to its internal structure had the best mechanical properties along the corrugation (WOLF *et al.*, 2021);
- honeycomb panels composed of two liners and a honeycomb core between them have a suitable structure for planar elements loaded perpendicularly to their surface (CRIPPS, 2004);
- paper board, best for use as an element that reinforces the properties of a building envelope or its finish;
- cellulose wool, and industrialised material providing thermal insulation to buildings, commonly used as a replacement for polystyrene and mineral wool.

As linear elements (paper tubes and cardboard profiles) are used as structural elements, their most significant feature is their mechanical properties, including bending and compression resistance. On the other hand, planar elements, that serve as partitions (external and internal) are subjected to loads, but also should have sufficient thermal and sound insulation.

The most critical properties of paper based products are their resistance to water and moisture, and incombustibility. However, there is a vast research conducted on those aspects of paper-based structures (KNAACK *et al.*, 2023). One of the least explored issues in the use of paper products in building structures is their acoustic properties. This is due to the focus of researchers on properties related to strength, fire and moisture effects and thermal insulation.

When comparing paper-based building partitions with traditional solutions, such as timber frame wall, it can be clearly seen that with similar thermal properties, products made of paper have a lower environmental impact (JASIOLEK *et al.*, 2023).

Paper can be therefore applied in both interior and exterior partitions. However, next to their structural, thermal and ecological properties, the sound insulation is one of the key features.

### 1.1. Acoustic characterisation of building materials

The fundamental acoustic attribute of regular building partitions is its potential impact on decreasing the noise imissions – either from external or internal sources. A complementary architectural design must fulfil the insulation requirements using components with known acoustic properties. The general building components used in partitions are not only sound insulators but also sound-absorbing materials applied as fillers of the structure. Each of these groups could be described by different parameters with corresponding measurement methods. Unfortunately, sustainable projects based on paper-based products are exacting because of inaccessibility to such data (LATKA *et al.*, 2022). Only sound-absorbing cellulose wool, as a material with growing use in both acoustic and thermal insulation, is sufficiently well-researched (ARENAS *et al.*, 2014). Hitherto published works on paper-based products included sound absorption and insulation tests of

corrugated cardboard (ASDRUBALI *et al.*, 2015; KANG *et al.*, 2021; LATKA, 2017a), honeycomb panels (SECHI *et al.*, 2016), paperboard (NERI *et al.*, 2021), and wastepaper (RICCIARDI *et al.*, 2014). Mentioned research, while valuable, could have a limited application in acoustic projects, either because the paper-based materials are a part of a bigger component, or the test is performed with a small sample impedance tube method.

This publication presents the acoustic parameters for cellulose wool and paper-based products: paperboard, corrugated cardboard, and honeycomb panels (unperforated and perforated). The conducted research employs three methods. First – the impedance tube transfer matrix method for the sound absorption coefficient  $\alpha$ , transmission loss (TL), the complex characteristic impedance  $z_c$ , and complex propagation wavenumber  $k$ , when possible. Second – the reverberation room method for the laboratory-tested weighted sound reduction index (SRI). Additionally, the beam resonance test was performed for paperboard exclusively to obtain its dynamic mechanical properties: Young's modulus  $E$  and the damping loss factor  $\eta$ .

## 2. Materials

The presented study examines the products (Fig. 1):

- cellulose wool made from recycled paper, with density varying from  $30 \text{ kg/m}^3$  to  $90 \text{ kg/m}^3$ ;
- recycled paperboard with the grammage of  $2000 \text{ g/m}^2$  and thickness of 3 mm;
- corrugated cardboard, types: BC, EE, EB, E, and B, as given in Table 1. The cardboard was measured in the configuration of a single plate or multiple plates:
  - a) five plates glued with polyvinyl acetate (PVA) adhesive (tested types are: EE, EB, and BC);
  - b) five plates stacked without any adhesive (tested types are: EE, BC, EE, and BC alternately).
- honeycomb plates with the different cells size, thicknesses and grammage, as listed in Table 2. The specific honeycomb geometry allows for enhancement of the absorption or insulation capabilities simply by perforating of the liner. Effectively, each cell transforms to the Helmholtz resonator with a resonance frequency dependent on the cell size, liner thickness and perforation diameter. Subsection 2.1 describes the concept of such a modification.

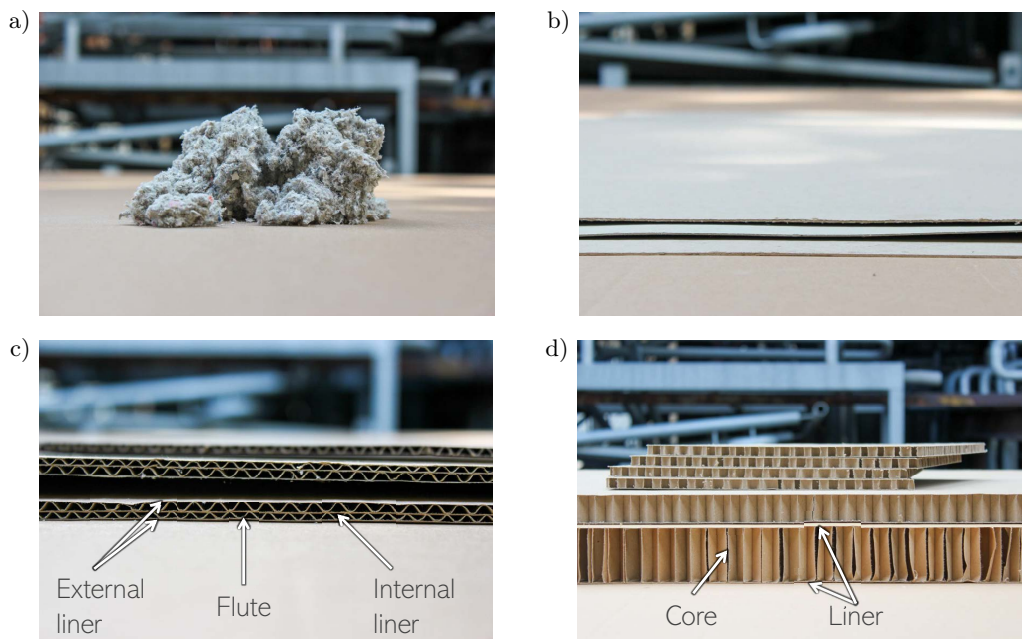


Fig. 1. Materials under test with their structure denotations: a) cellulose wool; b) paperboards; c) corrugated cardboards; d) honeycomb panels.

Table 1. Tested corrugated cardboard types and parameters.

Corrugated cardboard					
Thickness [mm]	Type	Grammage [ $\text{g/m}^2$ ]	Flute paper [ $\text{g/m}^2$ ]	External liner paper [ $\text{g/m}^2$ ]	Internal liner paper [ $\text{g/m}^2$ ]
6.1	Double wall BC	573	Wellenstoff 95	Testliner 110	Testliner 100
2.9	Double wall EE	555	Wellenstoff 95	Testliner 110	Testliner 100
4.0	Double wall EB	556	Wellenstoff 95	Testliner 110	Testliner 100
1.6	Single wall E	338	Wellenstoff 95	Testliner 110	–
2.7	Single wall B	342	Wellenstoff 95	Testliner 110	–

Table 2. Tested honeycomb panel types and parameters.

Honeycomb panels					
Symbol	Thickness [mm]	Cell size [mm]	Grammage [g/m <sup>2</sup> ]	Core paper [g/m <sup>2</sup> ]	Liner paper [g/m <sup>2</sup> ]
H50C22	50	22	1024	Testliner 120	Testliner 120
H50C14	50	14	1620	WB fluting 140	Testliner 120
H25C22	25	22	632	Testliner 120	Testliner 120
H25C14	25	14	930	WB fluting 140	Testliner 120
H10C10	10	10	590	WB fluting 140	Testliner 120
H50C22 KRAFT	50	22	1515	Testliber 140	Kraftliber 300
H25C22 KRAFT	25	22	1057	Testliber 140	Kraftliber 300

2.1. Honeycomb panels perforation

The honeycomb perforation creates the grid of Helmholtz resonators resulting in an exceedingly high absorption coefficient for the resonant frequency. Thus, the perforated honeycomb panels may be used as a filler for the existing structure to increase its sound insulation. May the double panel be the structure under examination in this case.

The resonance frequency  $f_R$  of the single Helmholtz resonator with a round neck is given by LANGFELDT *et al.* (2020):

$$f_R = \frac{c_0}{2\pi} \sqrt{\frac{S_R}{(l_R + \frac{\pi d_R}{4}) V_R}}, \tag{1}$$

where  $c_0$  is the speed of sound in air,  $S_R$ ,  $l_R$ ,  $d_R$ , and  $V_R$  are the resonator dimensions: cross-section surface, length, diameter of the neck, and volume of the cavity, respectively.

The mass-air-mass resonance frequency of air-filled double wall is (LANGFELDT *et al.*, 2020):

$$f_{DW} = \frac{1}{2\pi} \sqrt{\frac{K}{H} \left( \frac{1}{m''_1} + \frac{1}{m''_2} \right)}, \tag{2}$$

where  $K$  is the bulk modulus of air and  $H$  is the spacing between the walls with surface masses of  $m''_{1,2}$ .

LANGFELDT *et al.* (2020) proved that the resonance system of a double wall with the insertion of Helmholtz resonators has two resonance frequencies  $f_{01}$  and  $f_{02}$ , both different from but simultaneously dependent on  $f_R$  and  $f_{DW}$ :

$$f_{01,2}^2 = \frac{1 + \frac{f_R^2}{f_{DW}^2} \pm \sqrt{\left(1 - \frac{f_R^2}{f_{DW}^2}\right)^2 + 4\phi_R \frac{f_R^2}{f_{DW}^2}}}{2(1 - \phi_R)} f_{DW}^2 \tag{3}$$

with  $\phi_R$  being the volumetric fill ratio of Helmholtz resonators, in this case  $\phi_R = H_R/H$ , where  $H_R$  is

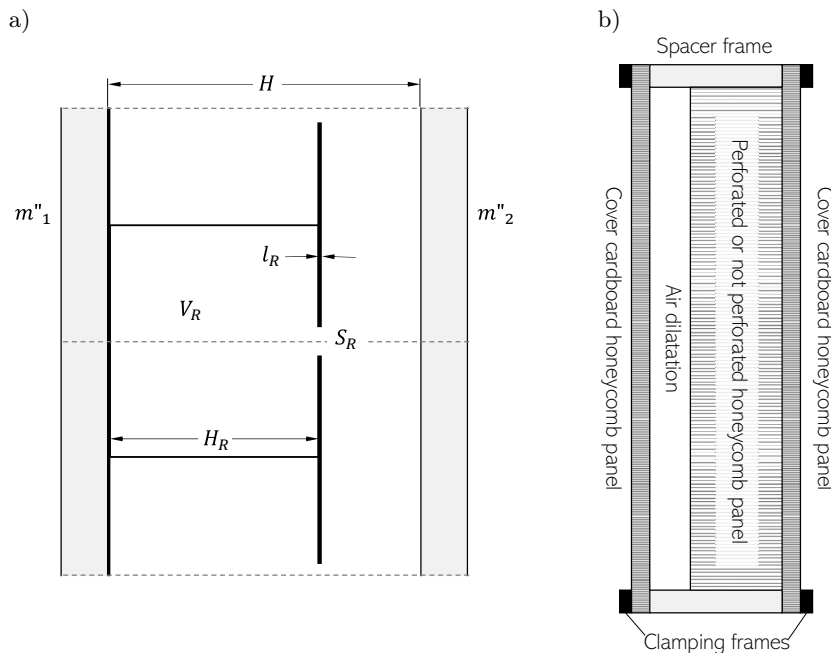


Fig. 2. Detailed scheme of the Helmholtz resonator in double wall (a) and schematic representation of a double wall with perforated or not perforated honeycomb cardboard insertion (b).

Table 3. Resonances frequencies of honeycomb panel perforation.

Honeycomb panel symbol	Assessed case	Neck diameter $d_R$ [mm]	Helmholtz resonance frequency $f_R$ [Hz]	Filling ratio $\phi_R$	Double wall resonance frequency $f_{DW}$ [Hz]	Resonance frequency $f_0$ (Eq. (3))	
						$f_{01}$ [Hz]	$f_{02}$ [Hz]
H50C22	Single panel	3.5	730	–	–	–	–
H25C22	Single panel	5	1260	–	–	–	–
H50C22 KRAFT	Double wall	1.8	316	0.725	346	247	725
H25C22 KRAFT	Double wall	1.6	416	0.625	474	325	1158

the height of the Helmholtz resonator cell (Fig. 2a). When  $f_R$  and  $f_{DW}$  are equal, Eq. (3) simplifies to:

$$f_0^2 = \frac{1 \pm \sqrt{\phi_R}}{1 - \phi_R} f_{DW}^2.$$

A significant transmission loss (TL) increase can be acquired in the bandwidth lying between given frequencies. The amplitude of this TL growth and its bandwidth depend on  $f_R$ ,  $f_{DW}$  and  $\phi_R$ . In case of the plane wave at an incidence angle  $\theta$ , the TL is represented by:

$$\begin{aligned} \text{TL} &= -10 \log \tau \\ &= -10 \log \left| \frac{2Z \sin(k_{\text{eff}} H \cos \theta_{\text{eff}})}{\mathcal{X}_1 \mathcal{X}_2 \sin^2(k_{\text{eff}} H \cos \theta_{\text{eff}}) + Z^2} \right|^2, \end{aligned} \quad (4)$$

where the effective wavenumber  $k_{\text{eff}} = 2\pi f \sqrt{\rho_{\text{eff}}/K_{\text{eff}}}$ , effective density  $\rho_{\text{eff}} \approx \rho_{\text{air}}(2 + \phi_R)/2(1 - \phi_R)$ , the angle of refraction  $\theta_{\text{eff}} = \arcsin(\sin \theta \sqrt{K_{\text{eff}}/\rho_{\text{eff}}/c_0})$ .

The angle related effective impedance is:

$$Z = Z_{\text{eff}} \sec \theta_{\text{eff}} / Z_{\text{air}} \sec \theta,$$

with the effective impedance  $Z_{\text{eff}} = \sqrt{K_{\text{eff}} \rho_{\text{eff}}}$ .

$$\mathcal{X}_{1,2} = X_{1,2} \cos \theta + 1 - Z \cot(k_{\text{eff}} H \cos \theta_{\text{eff}}),$$

where  $X_{1,2} = i\omega m''_{1,2}/Z_{\text{air}}$  are the normalized wall impedances. The factor  $K_{\text{eff}}$  is the effective bulk modulus of the Helmholtz resonator in closed volume as it is in the case under examination. For the damped ( $\zeta_R$  – resonator damping ratio) and air-filled system, the ratio  $K_{\text{eff}}$  to the air bulk modulus  $K$  is equal to:

$$\frac{K_{\text{eff}}}{K} = \frac{1}{1 - \phi_R + \frac{\phi_R}{1 + 2i\zeta_R \frac{\omega}{\omega_R} - \frac{\omega^2}{\omega_R^2}}}, \quad (5)$$

which means, that for certain frequencies  $f = \omega/2\pi$  above the Helmholtz resonance frequency  $f_R = \omega_R/2\pi$ , the  $K_{\text{eff}}$  could be lower below 0. This attribute – the negative bulk modulus (or the negative density, or both) is used in the acoustic metamaterial design, among other things, to increase sound insulation.

The diffused-field transmission coefficient could be then integrated over the incident angles from 0 to the maximum angle of  $\theta_l$ :

$$\bar{\tau} = \frac{\int_0^{\theta_l} \tau \cos \theta \sin \theta \, d\theta}{\int_0^{\theta_l} \cos \theta \sin \theta \, d\theta}. \quad (6)$$

The executed tests covered two issues: the sound absorption of a single perforated or non-perforated honeycomb panel and the sound reduction index of a double wall with the insertion of a perforated or non-perforated honeycomb panel, as in Fig. 2b. To match the Helmholtz resonance slightly below the double wall resonance, light honeycomb panels also form the covers. The dense honeycomb grid (H10C10 from Table 1) was chosen for this purpose, providing a small mass combined with high stiffness; and inhomogeneities, which do not influence the structure's vibration properties significantly. Table 3 lists all assessed structures along with their key parameters.

The analytically obtained results may differ in the practical applications. The cardboard production process does not guarantee the formation of equal cell volumes, which has two consequences: the change in width and position of the resonance (especially the width due to the resonance blur) and the technical difficulties in maintaining a constant opening position in relation to the cell. Both consequences do not exclude the honeycomb from potential utilization.

### 3. Methods

This paper employs three measurement methods:

- impedance tube two-loaded transfer function method (based on [ASTM E2611-19 \(2019\)](#)) for sound absorption coefficient  $\alpha$ , transmission loss TL, characteristic impedance  $z_c$ , and propagation wavenumber  $k$ ;
- laboratory measurements of sound insulation in a reverberation chamber (based on [International Organization for Standardization \(2000\)](#))

Table 4. Tested materials and used measurement methods with assessed parameters.

No.	Material	Sample thickness [mm]	Impedance tube measurement				Reverb. chamber measurement SRI (or $R_{I,M,W}$ )	Beam resonance measurement			
			$\alpha$	TL	$z_c$	$k'$		$E$	$\eta$		
1.	Cellulose wool made from recycled paper [kg/m <sup>3</sup> ]	Density 30	200	+	+	+	+	–	–	–	
		Density 40	200	+	+	+	+	–	–	–	
		Density 50	200	+	+	+	+	–	–	–	
		Density 60	200	+	+	+	+	–	–	–	
		Density 70	200	+	+	+	+	–	–	–	
		Density 80	200	+	+	+	+	–	–	–	
		Density 90	200	+	+	+	+	–	–	–	
2.	Paperboard – grammage 2000 g/m <sup>2</sup>	3.0	+	–	–	–	+	+	+		
3.	Corrugated cardboard	Type BC	6.1	–	–	–	–	+	–	–	
		Type EE	2.9	–	–	–	–	+	–	–	
		Type EB	4.0	–	–	–	–	+	–	–	
		Type E	1.6	–	–	–	–	+	–	–	
		Type B	2.7	–	–	–	–	+	–	–	
4.	Corrugated cardboard – five PVA glued layers	Type BC	30.5	–	–	–	–	+	–	–	
		Type EE	14.5	–	–	–	–	+	–	–	
		Type EB	20	–	–	–	–	+	–	–	
5.	Corrugated cardboard – five stacked layers	Type BC	30.5	–	–	–	–	+	–	–	
		Type EE	14.5	–	–	–	–	+	–	–	
		Type BC/EE	24.1	–	–	–	–	+	–	–	
6.	Honeycomb panel	H50C22	50	–	–	–	–	+	–	–	
		H50C14	50	–	–	–	–	+	–	–	
		H25C22	25	–	–	–	–	+	–	–	
		H25C14	25	–	–	–	–	+	–	–	
		H10C10	10	–	–	–	–	+	–	–	
		H50C22 KRAFT	50	+	+	–	–	–	+	–	–
		H25C22 KRAFT	25	+	+	–	–	–	+	–	–
7.	Perforated honeycomb panel*	H50C22 KRAFT	50	+	+	–	–	–	–	–	
		H25C22 KRAFT	25	+	+	–	–	–	–	–	
8.	Double wall with plain and perforated honeycomb panel*	H50C22	90	–	–	–	–	+	–	–	
		H25C22	60	–	–	–	–	+	–	–	

\* The perforation details are provided in Table 3.

for weighted modified intensity sound reduction index ( $R_{I,M,W}$ );

- measurement of vibration-damping properties with the beam resonance method (based on [ASTM E756-05 \(2005\)](#)) for dynamic Young's modulus  $E$  and the dynamic damping loss factor  $\eta$ .

Table 4 contains all tested materials assigned to the measurements performed upon them, along with assessed parameters.

### 3.1. Impedance tube two-loaded transfer function method

Two-loaded transfer function measurement was performed in an impedance tube system. The circular cross-section tube with an internal diameter of 101.7 mm was excited with the white noise. The tube parameter constrains the upper limit of the measured frequency range to 1600 Hz, thereby the results are provided for  $1/3$  octave bands in the range

50 Hz–1600 Hz. The digital audio pressure time processing determined the transfer function between the four individual microphones and created a transfer matrix. The Hanning window function was used to analyse the 10 s signal, resulting in a frequency resolution equal to 1 Hz. The used equipment were: power amplifier Atoll AM100SE, voltage output/input modules: NI 9260/NI 9234, and microphones G.R.A.S 46BD.

Three different specimens of each material were precisely trimmed to a diameter of 101.7 mm with a laser cutter, when possible. This operation allowed mounting them freely in the tube and consequently avoiding the emergence of membrane resonances in the range of the tested frequencies. Cellulose wool has been immobilized by two steel grids not affecting the acoustic field (Fig. 3a). Any leaks between the pipe and the plates were sealed with butyl.

The [ASTM E2611-19 \(2019\)](#) refers to the normal incidence sound transmission loss measurement, however it also outlines procedures for measuring other

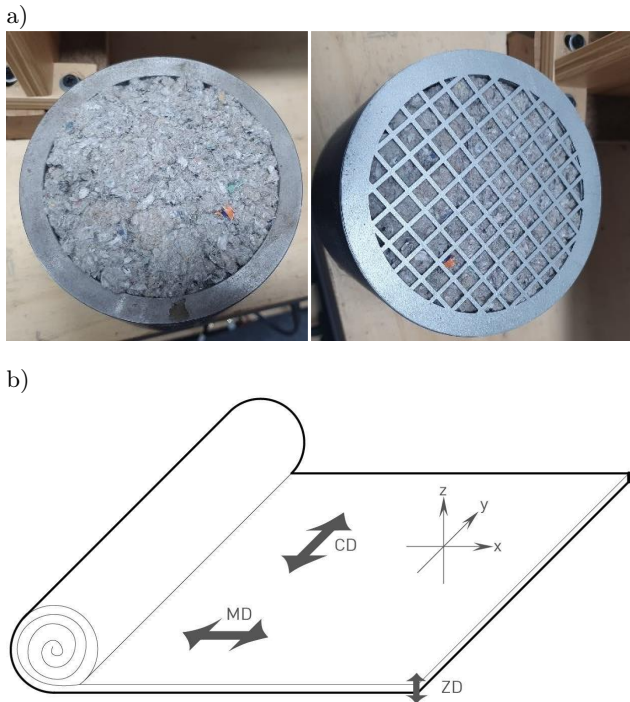


Fig. 3. a) Cellulose wool mounting; b) production directions of paperboard: machine direction (MD); cross-machine direction (CD); thickness direction (ZD) (NISKANEN, 2011).

material properties, employing the transfer matrix method. As a result, the relationship for determining the hard-backed absorption coefficient is provided as:

$$\alpha = 1 - |R|^2 = 1 - \left| \frac{T_{11} - \rho_0 c_0 T_{21}}{T_{11} + \rho_0 c_0 T_{21}} \right|^2, \quad (7)$$

where  $R$  – the hard backed reflection coefficient,  $\rho_0$ ,  $c_0$  – density and sound speed in air,  $T_{ii}$  – measured transfer matrix elements (see ASTM E2611-19 (2019) for details).

Correspondingly, the complex propagation wave-number  $k'$  and the complex characteristic impedance  $z_c$  are given by

$$k' = \frac{1}{d} - \cos^{-1} T_{11} \quad (8)$$

and

$$z = \sqrt{\frac{T_{12}}{T_{21}}}, \quad (9)$$

where  $d$  is the thickness of a sample.

### 3.2. Laboratory measurements of sound insulation in a reverberation chamber

The subsequent reverberation chamber measurement delivered the resulting weighted modified intensity sound reduction index  $R_{I,M,W}$  along with the correction factors  $C$  and  $C_{tr}$ . The measurement consisted in clamping a sample with dimensions of

1162 mm × 865 mm in the window of the reverberation transmitting chamber with a volume of 67 m<sup>3</sup> and non-parallel walls. The joint between the clamping frame and the sample was sealed with butyl and a layer of EPDM rubber. The chamber was excited by a reference sound source Norsonic 276 positioned to create a diffuse sound field, whose average sound pressure level was then measured by a sound level meter SV 22 at locations representative of the sound energy impacting the sample. The sound intensity probe measured the signal outside the chamber with a sweeping method. The Gras 40GK 1/2'' microphones being part of the sound intensity probe were located at a 100 mm distance from the sample surface. The used probe microphone separator was 50 mm.

The measurements were unfortunately confined to 1/3 octave bands in the range of 100 Hz–1600 Hz. The lower limit was a result of resonances occurring within the reverberation chamber, leading to its misalignment with the low-frequency range. The upper limit aligns with the range of the utilized probe separator. Consequently, the SRI values for frequencies between 1600 Hz and 3150 Hz are absent from the following graphs, though they have been factored into the weighted SRI and spectrum adaptation terms. This decision was taken for three main reasons: first, the observed values followed the trend established by the previous frequency bands and adhered to pertinent physical laws (e.g., mass law). Second, the PI index condition was satisfied for all results. Finally, even significant fluctuations in these three bands' values (by ±3 dB) did not induce changes in the calculated parameters exceeding 1 dB. Nonetheless, it should be noted that the concerned parameters are only approximated.

### 3.3. Beam resonance method for vibration-damping properties

The dynamic mechanic properties are essential to perform numerous computer acoustic analyses, i.e., widely used the finite element analyses (FEA). Paperboard, as a non-linear material, has vastly different values for dynamic properties than static ones. What is more, due to the production process, paperboard is an orthogonal material with machine direction (MD) properties incomparable to the cross-machine direction (CD) (Fig. 3b). Thus, the tests apply to both MD and CD directions and for several vibration frequency points between 30 Hz and 160 Hz.

The beam resonance method measures the frequency and the quality factor of cantilever beam resonance. In this examination, the used method is completely non-contact, meaning the beam vibration velocity was obtained with a Polytec PSV-400 laser vibrometer, while the beam itself was excited by a Brüel & Kjær MM002 magnetic transducer with chirp signal.

The transducer affected a metal plate with a negligible mass, attached to the beam by synthetic wax.

This configuration makes it possible to determine the dynamic Young modulus  $E$ , for the resonance frequency of the 1st mode  $f$ , as in (ASTM E756-05 (2005)):

$$E = \frac{(12\rho l^4 f^2)}{(H_b^2 C_1^2)}, \quad (10)$$

and the damping loss factor as:

$$\eta = \frac{\Delta f}{f}, \quad (11)$$

where  $\rho$  – volumetric density,  $l$  – beam length,  $H_b$  – beam height in the vibration direction,  $C_1$  – coefficient for the mode 1 of the clamped-free beam, equal 0.55959,  $\Delta f$  – half-power bandwidth.

#### 4. Results and discussion

This section presents the results divided by the material groups, as in Table 4, of the methods described in Sec. 3:

1. cellulose wool made from recycled paper;
2. paperboard;
- 3.–5. corrugated cardboard – single plates and multiple layers;
- 6.–8. honeycomb panel – single plates and structures with and without perforation.

##### 4.1. Cellulose wool

Cellulose wool is a loose material widely used in building insulation as an alternative to mineral wool or fibreglass. The wool under examination is a commercial product used for this purpose, i.e. it contains flame retardant and anti-moisture additives. Wool, as a fibrous material, has been tested for a wide range of acoustic properties. Apart from the sound absorption and transmission loss, the characteristic impedance  $z_c$ , and the propagation wavenumber  $k'$  are also the subject of this study.

Figure 4 shows the first two parameters' results for several wool densities. For the lowest density of  $30 \text{ kg/m}^3$  and material thickness equal to 20 cm, the sound absorption coefficient reaches 1, by a frequency of 250 Hz. For the mentioned thickness, the sound absorption worsens above the density of  $50 \text{ kg/m}^3$ . The cellulose wool has similar absorption properties to conventional materials, which similarity is particularly visible in comparison to fibreglass in Fig. 5. Simultaneously, recycled materials such as cellulose wool have a significantly lower environmental impact. For instance – cellulose fibre has over 2.5 times smaller primary energy demand, over 1.5 smaller water demand, and a similar Global Warming Potential to rock wool with the same mass (ZABALZA BRIBIÁN *et al.*, 2011).

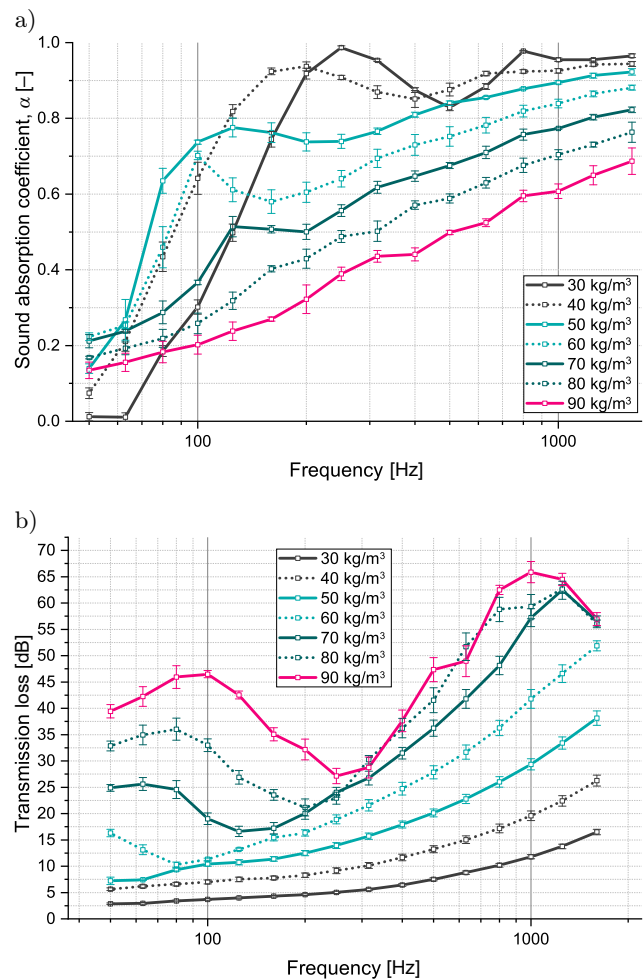


Fig. 4. Results of the sound absorption coefficient (a) and transmission loss (b) of different densities recycled cellulose wool. Horizontal lines mark standard error of measurements.

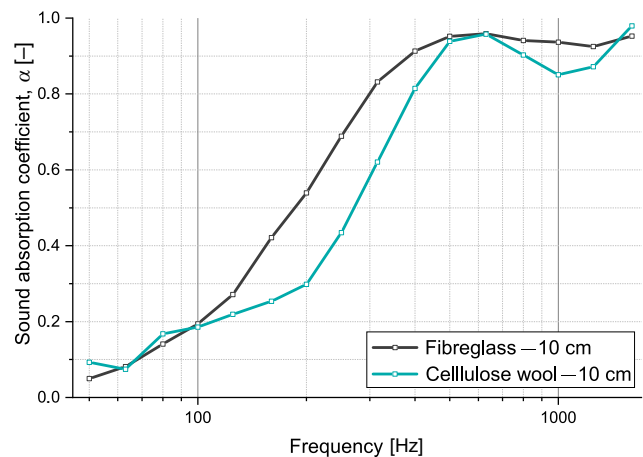


Fig. 5. Sound absorption coefficient comparison of the same density and thickness recycled cellulose wool (blue) and fibreglass (black) ( $30 \text{ kg/m}^3$ ). The results for cellulose wool were calculated with the data available in Table 5.

Table 5 presents the values of the characteristic impedance  $z$  and propagation factor  $k'$ . The data is



Table 5. Results of the complex characteristic impedance  $z_c$  [kg/m<sup>2</sup>s] and complex propagation wavenumber  $k'$  [1/m] of recycled cellulose wool.

Density [kg/m <sup>3</sup> ]	Parameter	The centre frequency of the 1/3 octave band [Hz]																
		50	63	80	100	125	160	200	250	315	400	500	630	800	1000	1250	1600	
30	$\Re(z_c) \pm \sigma$	926 ± 14	837 ± 9	825 ± 7	799 ± 7	770 ± 5	735 ± 5	705 ± 5	676 ± 5	652 ± 7	646 ± 10	669 ± 14	667 ± 11	618 ± 9	602 ± 12	603 ± 15	598 ± 14	
	$\Im(z_c) \pm \sigma$	-344 ± 18	-329 ± 13	-259 ± 15	-241 ± 11	-213 ± 9	-185 ± 8	-161 ± 7	-140 ± 6	-118 ± 4	-92 ± 4	-78 ± 2	-84 ± 5	-74 ± 6	-56 ± 8	-22 ± 6	-12 ± 9	-12 ± 9
	$\Re(k') \pm \sigma$	7.3 ± 0.1	7.3 ± 0.1	7.3 ± 0.1	7.3 ± 0.1	7.3 ± 0.1	7.3 ± 0.1	7.4 ± 0.1	8.8 ± 0.1	10.6 ± 0.1	13 ± 0.1	13 ± 0.1	15.7 ± 0.1	19.1 ± 0.1	23.5 ± 0.1	28.5 ± 0.2	34.5 ± 0.2	42.9 ± 0.2
	$\Im(k') \pm \sigma$	-2.2 ± 0.1	-2.2 ± 0.1	-2.2 ± 0.1	-2.2 ± 0.1	-2.2 ± 0.1	-2.2 ± 0.1	-2.2 ± 0.1	-2.6 ± 0.1	-3 ± 0.1	-3.5 ± 0.1	-3.5 ± 0.1	-4.1 ± 0.2	-4.8 ± 0.2	-5.7 ± 0.2	-6.7 ± 0.2	-7.8 ± 0.2	-9.4 ± 0.3
	$\Re(z_c) \pm \sigma$	1176 ± 29	1097 ± 22	1066 ± 19	1025 ± 12	967 ± 12	890 ± 27	832 ± 33	772 ± 41	737 ± 39	735 ± 26	746 ± 15	736 ± 11	695 ± 9	675 ± 12	662 ± 14	653 ± 19	653 ± 19
40	$\Im(z_c) \pm \sigma$	-621 ± 26	-577 ± 23	-497 ± 24	-466 ± 34	-430 ± 37	-378 ± 32	-330 ± 22	-278 ± 12	-221 ± 11	-180 ± 21	-164 ± 20	-145 ± 18	-123 ± 20	-113 ± 19	-72 ± 16	-55 ± 18	-55 ± 18
	$\Re(k') \pm \sigma$	6.2 ± 0.3	6.2 ± 0.3	6.2 ± 0.3	6.2 ± 0.3	6.2 ± 0.3	6.2 ± 0.3	6 ± 0.3	4.6 ± 0.2	2.4 ± 0.2	0.3 ± 0.2	3.4 ± 0.2	7.3 ± 0.2	12.3 ± 0.2	17.9 ± 0.3	24.6 ± 0.3	33.9 ± 0.3	33.9 ± 0.3
	$\Im(k') \pm \sigma$	-4.2 ± 0.3	-4.2 ± 0.3	-4.2 ± 0.3	-4.2 ± 0.3	-4.2 ± 0.3	-4.2 ± 0.3	-4.3 ± 0.3	-4.9 ± 0.4	-5.5 ± 0.4	-6.4 ± 0.4	-7.2 ± 0.4	-8.3 ± 0.4	-9.6 ± 0.5	-11 ± 0.5	-12.6 ± 0.6	-14.9 ± 0.6	-14.9 ± 0.6
	$\Re(z_c) \pm \sigma$	1017 ± 13	1246 ± 77	1403 ± 55	1345 ± 67	1234 ± 62	1135 ± 45	1033 ± 34	946 ± 16	887 ± 17	854 ± 15	839 ± 4	819 ± 12	772 ± 21	742 ± 28	721 ± 29	706 ± 30	706 ± 30
	$\Im(z_c) \pm \sigma$	-967 ± 158	-714 ± 60	-706 ± 22	-740 ± 43	-686 ± 59	-610 ± 51	-546 ± 56	-462 ± 47	-391 ± 24	-340 ± 4	-301 ± 17	-251 ± 23	-205 ± 22	-183 ± 18	-125 ± 17	-88 ± 13	-88 ± 13
50	$\Re(k') \pm \sigma$	3.6 ± 0.2	3.6 ± 0.2	3.6 ± 0.2	3.6 ± 0.2	3.6 ± 0.2	3.6 ± 0.2	3.3 ± 0.2	1.5 ± 0.2	1 ± 0.3	4.2 ± 0.3	7.7 ± 0.3	12 ± 0.3	17.5 ± 0.3	23.7 ± 0.3	31.1 ± 0.2	41.3 ± 0.2	41.3 ± 0.2
	$\Im(k') \pm \sigma$	-6.2 ± 0.3	-6.2 ± 0.3	-6.2 ± 0.3	-6.2 ± 0.3	-6.2 ± 0.3	-6.2 ± 0.3	-6.3 ± 0.3	-7.2 ± 0.3	-8.4 ± 0.4	-9.7 ± 0.4	-11 ± 0.4	-12.6 ± 0.5	-14.5 ± 0.5	-16.5 ± 0.6	-18.8 ± 0.6	-21.6 ± 0.7	-21.6 ± 0.7
	$\Re(z_c) \pm \sigma$	1327 ± 92	1211 ± 77	1339 ± 107	1615 ± 157	1569 ± 120	1373 ± 92	1255 ± 94	1182 ± 77	1096 ± 68	1032 ± 52	994 ± 38	959 ± 26	899 ± 17	858 ± 18	833 ± 19	808 ± 20	808 ± 20
	$\Im(z_c) \pm \sigma$	-2089 ± 140	-1593 ± 146	-992 ± 144	-898 ± 17	-948 ± 40	-886 ± 60	-724 ± 50	-638 ± 52	-561 ± 51	-504 ± 55	-446 ± 55	-368 ± 51	-295 ± 45	-261 ± 40	-185 ± 35	-133 ± 30	-133 ± 30
	$\Re(k') \pm \sigma$	0.8 ± 0.5	0.8 ± 0.5	0.8 ± 0.5	0.8 ± 0.5	0.8 ± 0.5	0.8 ± 0.5	0.5 ± 0.5	2 ± 0.6	5 ± 0.6	8.7 ± 0.5	12.8 ± 0.5	17.6 ± 0.5	23.8 ± 0.5	30.2 ± 0.5	38.8 ± 0.6	44.3 ± 8.7	44.3 ± 8.7
60	$\Im(k') \pm \sigma$	-7.8 ± 0.3	-7.8 ± 0.3	-7.8 ± 0.3	-7.8 ± 0.3	-7.8 ± 0.3	-7.8 ± 0.3	-8 ± 0.2	-9.4 ± 0.3	-11.2 ± 0.5	-13.1 ± 0.6	-15 ± 0.6	-17.3 ± 0.7	-20.1 ± 0.8	-23.3 ± 1	-26.1 ± 0.9	-29.3 ± 0.5	-29.3 ± 0.5
	$\Re(z_c) \pm \sigma$	1959 ± 70	1920 ± 77	1671 ± 114	1529 ± 121	1568 ± 90	1588 ± 78	1579 ± 71	1367 ± 58	1300 ± 46	1219 ± 33	1178 ± 21	1144 ± 11	1078 ± 7	1035 ± 8	1005 ± 9	972 ± 10	972 ± 10
	$\Im(z_c) \pm \sigma$	-3146 ± 136	-2783 ± 139	-2284 ± 71	-1793 ± 32	-1393 ± 49	-1084 ± 54	-1033 ± 46	-933 ± 49	-741 ± 54	-687 ± 55	-591 ± 51	-479 ± 47	-369 ± 43	-326 ± 37	-223 ± 33	-154 ± 30	-154 ± 30
	$\Re(k') \pm \sigma$	2 ± 0.6	2 ± 0.6	2 ± 0.6	2 ± 0.6	2 ± 0.6	2 ± 0.6	2.4 ± 0.7	5.3 ± 0.7	8.8 ± 0.7	13.8 ± 0.7	18.3 ± 0.7	24.1 ± 0.7	31.1 ± 0.7	40.1 ± 0.7	60.1 ± 4.3	58.6 ± 15.7	58.6 ± 15.7
	$\Im(k') \pm \sigma$	-8.5 ± 0.3	-8.5 ± 0.3	-8.5 ± 0.3	-8.5 ± 0.3	-8.5 ± 0.3	-8.5 ± 0.3	-8.8 ± 0.3	-11.3 ± 0.3	-12.8 ± 0.5	-15.7 ± 0.6	-18.3 ± 0.6	-21.5 ± 0.8	-25.4 ± 0.8	-30.6 ± 0.9	-33.6 ± 0.8	-31.1 ± 0.5	-31.1 ± 0.5
70	$\Re(z_c) \pm \sigma$	2370 ± 106	2436 ± 123	2210 ± 119	2019 ± 133	1806 ± 113	1670 ± 88	1647 ± 85	1712 ± 69	1533 ± 54	1421 ± 41	1393 ± 29	1350 ± 22	1271 ± 17	1217 ± 20	1171 ± 23	1128 ± 15	1128 ± 15
	$\Im(z_c) \pm \sigma$	-4111 ± 138	-3660 ± 73	-3131 ± 87	-2661 ± 38	-2179 ± 46	-1647 ± 58	-1208 ± 51	-1088 ± 56	-1090 ± 55	-863 ± 55	-798 ± 51	-629 ± 49	-476 ± 41	-425 ± 35	-292 ± 33	-188 ± 26	-188 ± 26
	$\Re(k') \pm \sigma$	0.7 ± 0.4	0.7 ± 0.4	0.7 ± 0.4	0.7 ± 0.4	0.7 ± 0.4	0.8 ± 0.5	1.6 ± 0.5	8 ± 0.5	15 ± 0.5	17.9 ± 0.5	26.7 ± 0.4	32.3 ± 0.4	40.4 ± 0.5	51.7 ± 3.5	64.3 ± 8.2	61.1 ± 16.9	61.1 ± 16.9
	$\Im(k') \pm \sigma$	-8.4 ± 0.2	-8.4 ± 0.2	-8.4 ± 0.2	-8.4 ± 0.2	-8.4 ± 0.2	-8.4 ± 0.2	-8.4 ± 0.2	-9.6 ± 0.2	-14.5 ± 0.3	-17.4 ± 0.3	-20.4 ± 0.4	-26.1 ± 0.5	-30.6 ± 0.7	-31.3 ± 0.6	-34.3 ± 0.5	-30.6 ± 0.2	-30.6 ± 0.2
	$\Re(z_c) \pm \sigma$	3347 ± 88	3630 ± 101	3420 ± 98	3312 ± 110	3043 ± 92	2696 ± 70	2383 ± 71	2142 ± 58	1950 ± 35	1781 ± 25	1807 ± 19	1645 ± 16	1594 ± 17	1543 ± 18	1435 ± 13	1435 ± 13	1435 ± 13
80	$\Im(z_c) \pm \sigma$	-5038 ± 154	-4757 ± 78	-4126 ± 85	-3645 ± 39	-3116 ± 55	-2558 ± 52	-2079 ± 54	-1577 ± 54	-1279 ± 57	-1242 ± 57	-1002 ± 53	-848 ± 44	-596 ± 40	-531 ± 35	-364 ± 33	-234 ± 25	-234 ± 25
	$\Re(k') \pm \sigma$	2.6 ± 0.5	2.6 ± 0.5	2.6 ± 0.5	2.6 ± 0.5	2.6 ± 0.5	2.6 ± 0.5	2.2 ± 0.5	3.1 ± 0.6	13.2 ± 0.5	23 ± 0.5	27.5 ± 0.6	38.2 ± 0.5	51.2 ± 0.6	51.8 ± 0.6	73.4 ± 2.6	55.8 ± 9.2	55.8 ± 9.2
	$\Im(k') \pm \sigma$	-13.4 ± 0.3	-13.4 ± 0.3	-13.4 ± 0.3	-13.4 ± 0.3	-13.4 ± 0.3	-13.4 ± 0.3	-13.1 ± 0.4	-10.5 ± 0.5	-11.3 ± 0.7	-16.3 ± 0.8	-22.1 ± 0.8	-22.6 ± 0.9	-31.9 ± 1.1	-33.2 ± 1.1	-33.5 ± 0.7	-29.7 ± 0.4	-29.7 ± 0.4

tabular, thanks to which it can be managed with ease. The possible applications are, among others, acoustic computer modelling of the equivalent fluid model or estimating the dimension dependent acoustic parameters. In this manner, the sound absorption coefficient  $\alpha$  for the thinner, 10 cm cellulose wool layer, visible in Fig. 4. was calculated with (COX, D'ANTONIO, 2016):

$$\alpha = 1 - \left| \frac{\frac{z_1}{\rho_0 c_0} \cos \psi - 1}{\frac{z_1}{\rho_0 c_0} \cos \psi + 1} \right|^2, \quad (12)$$

where  $z_1$  – rigid back absorbent surface impedance,  $z_1 = jz_c \cot(kd_1)$ ,  $d_1$  – layer thickness,  $\rho_0 c_0$  – air acoustic impedance,  $\psi$  – incidence angle of the wave.

#### 4.2. Paperboard

The single sheet of paperboard with a grammage of 2000 g/m<sup>2</sup> and a thickness of 3 mm has SRI equal to 13 dB and sound absorption not exceeding 0.05 over the whole frequency range (Fig. 6).

The dynamic Young Modulus is approximately 2.3 GPa for the machine direction and 1.1 GPa for the

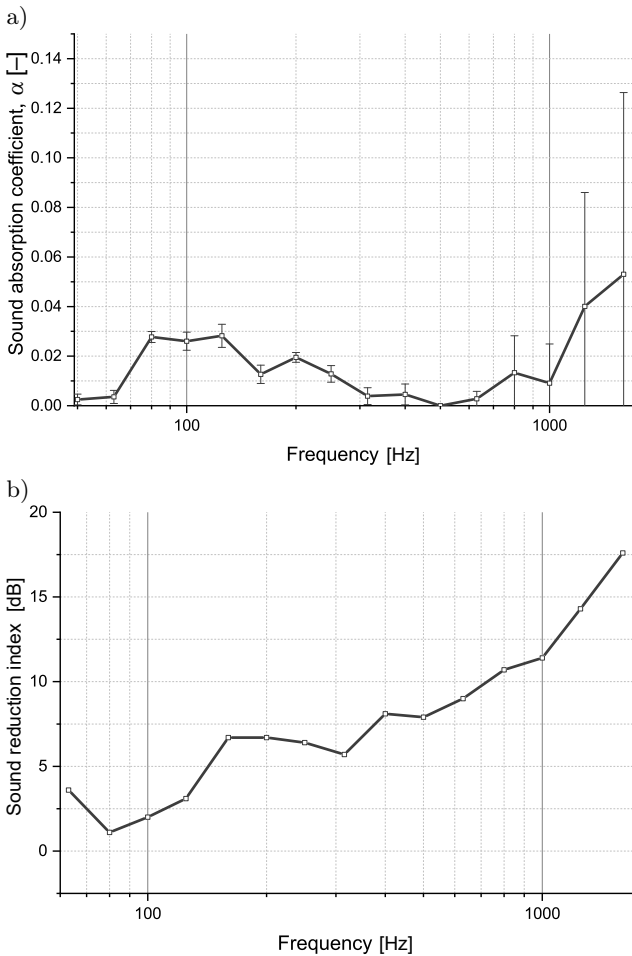


Fig. 6. Results of 2000 g/m<sup>2</sup> paperboard acoustic properties: a) sound absorption coefficient with standard error marked with horizontal lines; b) sound reduction index.

cross-machine direction and decreases slightly with frequency (Fig. 7). The disproportion between the directions is also visible in the repeatability of the results – the CD measurements are stable, which cannot be claimed in the second case, especially for lower frequencies. Both observations are easily explainable by the papermaking process: the pressure forces fibres to align parallelly to the machine direction, leading to higher elasticity and greater density unevenness. The literature provides higher values for static Young's Modulus – 5.4 GPa for MD, 1.9 GPa for CD (NISKANEN, 2011) or 2 GPa–20 GPa for MD, 0.5 GPa–10 GPa for CD (SCHÖNWÄLDER, ROTS, 2008). Unfortunately, a direct comparison is impossible, as there is no data about the paperboard dimensions or density, which may greatly impact the values. Damping properties are less correlated to frequency, e.g., for CD, the Pearson correlation coefficient is –0.67 (while for Young's Modulus, it reaches –0.98). The ratio is also direction-independent, i.e., the mean value equals 0.034 for MD and 0.036 for CD.

The acquired values suggest that in an accurate dynamic model of the paperboard, Young's Modulus

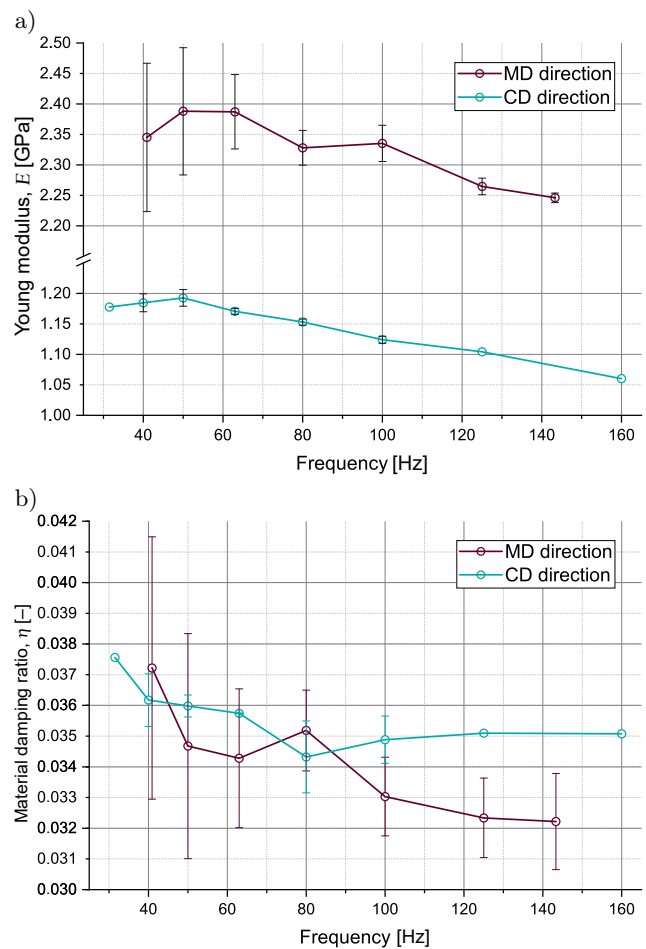


Fig. 7. Results of dynamic Young's Modulus (a) and damping ratio (b) of paperboard with grammage of 2000 g/m<sup>2</sup>. Horizontal lines mark standard error of measurements.

values should relate to the frequency, while damping can be represented by a single value.

### 4.3. Corrugated cardboard

A single wall corrugated cardboard panel have a SRI of 7 dB (for type B) and 9 dB (for type E). Despite the comparable surface mass, the second type reaches a noticeably larger value, most likely due to its more compact structure. This difference disappears when introducing the additional wall – the EE, EB, and BC plates have SRI equal to 11 dB, 12 dB, and 12 dB, respectively (Fig. 8).

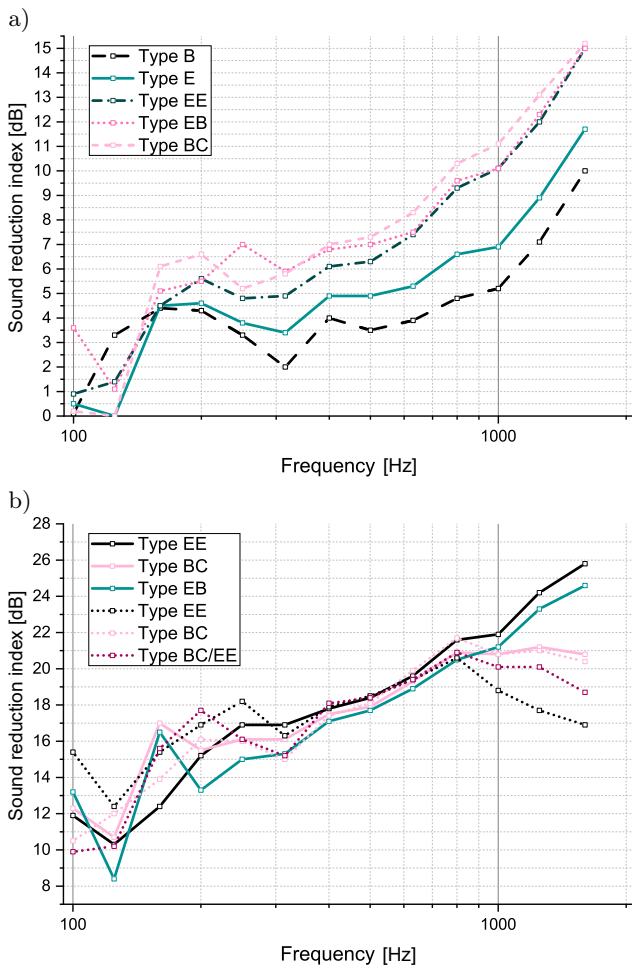


Fig. 8. Results of the sound reduction index of corrugated cardboard: a) the single plate with 3 layers (dashed lines) or 5 layers (solid lines); b) composition of 5 plates stacked without an adhesive (dotted lines) or glued with PVA (solid lines).

The multiple layered samples were arranged with flutes oriented parallel to each other. The stacked panels (Fig. 8) had no adhesive on any part of the surface. The amount of PVA adhesive used in the second case was 150 g/m<sup>2</sup>, which had an imperceptible effect on the total weight after drying. The SRI in each case is remarkably similar and ranges from 19 dB to 22 dB (see Table 6). As with the double-wall panel, the flute

type has negligible impact on the results, even if the most compact EE layers are arranged alternately with thick BC layers. The only distinction between the results lies above the 1000 Hz, where the SRI of stacked panels decreases rapidly.

The overall insulation property of a 5-layered structure is relatively high, especially when compared to a very low surface mass of the whole structure, which is about 2.8 kg/m<sup>2</sup>. The resulting SRI could match the properties of heavier walls, for example, a double 3 mm beaverboard panel with a filling of 30 mm Styrofoam and SRI equal to 21 dB has more than twice the surface mass of 6 kg/m<sup>2</sup> (ŁATKA et al., 2022).

### 4.4. Honeycomb panels

The SRI of honeycomb panels is consistent with the law of mass and similar for almost all cases (Table 6). Heavier Kraftliber sheets have a weighted index higher by 2 dB than the corresponding panels of

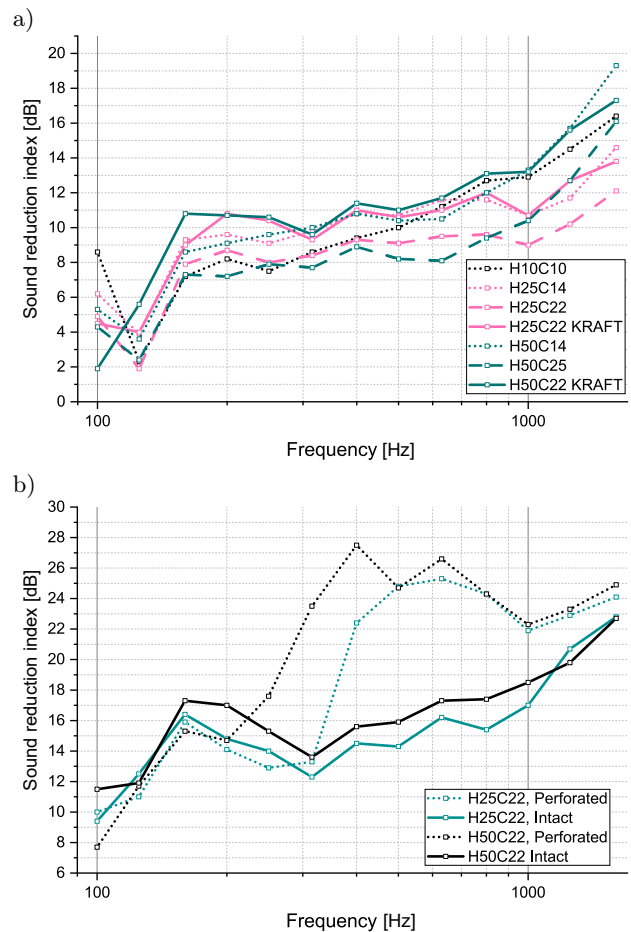


Fig. 9. Sound reduction index of honeycomb panels: a) comparison of different single panel types. Dotted lines: dense structures with cell size of 10 mm and 14 mm, dashed lines: lightweight structures with cell size of 22 mm, solid lines: Kraftliber structures with cell size of 22 mm; b) the influence of perforations on the double wall insulation. Dotted lines: perforated honeycomb insertion, solid lines: unperforated honeycomb insertion.

Table 6. Tested materials and used measurement methods with assessed parameters.

No.	Material	Thickness [mm]	Surface mass [kg/m <sup>2</sup> ]	Weighted SRI* [dB]	Spectrum adaption terms [dB]		Average sound absorption coefficient**	
					C*	C <sub>tr</sub> *		
1.	Cellulose wool made from recycled paper [kg/m <sup>3</sup> ]	Density 30	200	6.0	–	–	–	0.93
		Density 40	200	8.0	–	–	–	0.91
		Density 50	200	10.0	–	–	–	0.84
		Density 60	200	12.0	–	–	–	0.76
		Density 70	200	14.0	–	–	–	0.69
		Density 80	200	16.0	–	–	–	0.61
		Density 90	200	18.0	–	–	–	0.52
2.	Paperboard	3.0	2.0	<b>13</b>	–1	–3	0.03	
3.	Corrugated cardboard	Type BC	6.1	0.5	<b>12</b>	–1	–3	–
		Type EE	2.9	0.6	<b>11</b>	0	–2	–
		Type EB	4.0	0.6	<b>12</b>	–1	–3	–
		Type E	1.6	0.3	<b>9</b>	–1	–2	–
		Type B	2.7	0.3	<b>7</b>	0	–2	–
4.	Corrugated cardboard – five PVA glued layers	Type BC	30.5	2.7	<b>20</b>	–1	–1	–
		Type EE	14.5	2.8	<b>21</b>	–1	–3	–
		Type EB	20	2.8	<b>22</b>	–1	–3	–
5.	Corrugated cardboard – five stacked layers	Type BC	30.5	2.7	<b>21</b>	–1	–2	–
		Type EE	14.5	2.8	<b>19</b>	0	–1	–
		Type BC/EE	24.1	2.8	<b>20</b>	–1	–2	–
6.	Honeycomb panel	H50C22	50	1.0	<b>13</b>	–1	–3	–
		H50C14	50	1.6	<b>15</b>	0	–3	–
		H25C22	25	0.6	<b>11</b>	0	–1	–
		H25C14	25	0.9	<b>13</b>	0	–2	–
		H10C10	10	0.6	<b>14</b>	–1	–2	–
		H50C22 KRAFT	50	1.5	<b>15</b>	0	–2	0.14
		H25C22 KRAFT	25	1.1	<b>13</b>	0	–2	0.19
7.	Perforated honeycomb panel	H50C22 KRAFT	50	1.5	–	–	–	0.59
		H25C22 KRAFT	25	1.1	–	–	–	0.44
8.	Double wall with intact and perforated honeycomb panel	H50C22 Intact	90	2.2	<b>20</b>	0	–2	–
		H25C22 Intact	40	1.8	<b>19</b>	0	–2	–
		H50C22 Perforated	90	2.2	<b>26</b>	–2	–5	–
		H25C22 Perforated	40	1.8	<b>23</b>	–1	–3	–

\* Weighted sound reduction index and spectrum adaption terms are approximated. See Subsec. 3.2 for explanation.

\*\* For 1/3 octave bands 200 Hz ÷ 1600 Hz.

the same geometry (15 dB versus 13 dB for a thickness of 50 mm and 13 dB versus 11 dB for a thickness of 25 mm). The exact rule applies to the core mass increase. By reducing the cell size, the surface gains an additional 1/3 of its mass and 2 dB in insulation. The panel with the finest structure (H10C10) breaks this dependency with the SRI equal to 14 dB. This value is close to the performance of almost three times heavier panels (H50C22 with Kraftliber and H50C14). The frequency-dependent increase of SRI is more rapid for the H10C10 panel, thus it reaches an exceptionally high value for frequencies above 500 Hz (Fig. 9). This increase may correlate to the resonances arising in a denser structure.

As described in Subsec. 2.1, the honeycomb perforation efficiently improves its acoustic parameters.

The average sound absorption coefficient in the 1/3 octave band for a single panel (Fig. 10a), reaches the values:

- 0.98 for the H50C22 KRAFT sample. The calculated frequency of 730 Hz fits the reported band of 800 Hz;
- 0.90 for the H25C22 KRAFT sample. In this case, the frequency of 1260 Hz also corresponds to the observed 1250 Hz.

The perforation induced a slight reduction in transmission loss, equalling 2 dB–3 dB in the whole frequency band (Fig. 10b).

Figure 9b displays the improvement in the sound reduction index of the honeycomb double wall with the perforated insertion over the intact one (as proposed in Fig. 2b). In the case of panel H25C22, the rapid insulation increase is observable from the 400 Hz frequency

band and results in an overall 4 dB gain in full-band weighted SRI (from 19 dB to 23 dB Table 6). The improvement of H50C22 insertion is even more substantial. The growth is visible from the 315 Hz frequency band and causes a weighted SRI shift from 20 dB to 26 dB. Unfortunately, since the gain is achieved only in part of the whole frequency range, both Spectrum Adaption Terms (C and Ctr) deteriorate by 1 dB–3 dB.

The SRI increase is compared to the analytical result in Fig. 11. The calculations were performed with the following assumptions:

- the insertion moves with the cover panel (its weight is calculated to the cover wall);
- the distance between the double walls is reduced by insertion panel thickness in an intact case;
- the Helmholtz resonator damping ratio is 0.2;
- the probe was affected by the diffused field, with waves incident at the angle range from  $0^\circ$  to  $80^\circ$ .

The analytical model aligns very well with the experiment result, proving that the perforated honeycomb panel can be successfully represented by the proposed analytical model.

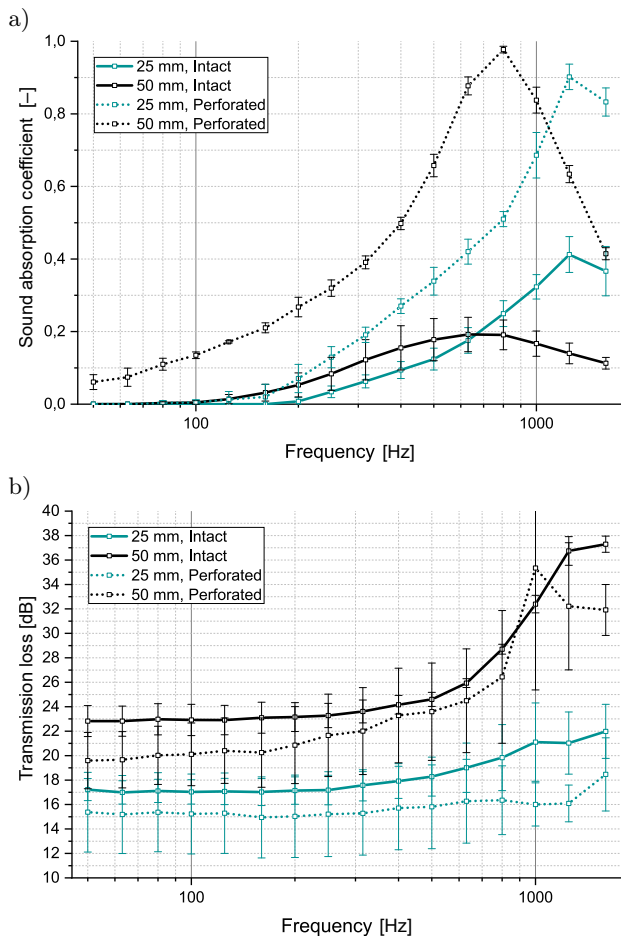


Fig. 10. The results of the sound absorption coefficient (a) and transmission loss (b) of single plate honeycomb panel, with (dotted lines) or without (solid lines) perforation. Horizontal lines mark standard error of measurements.

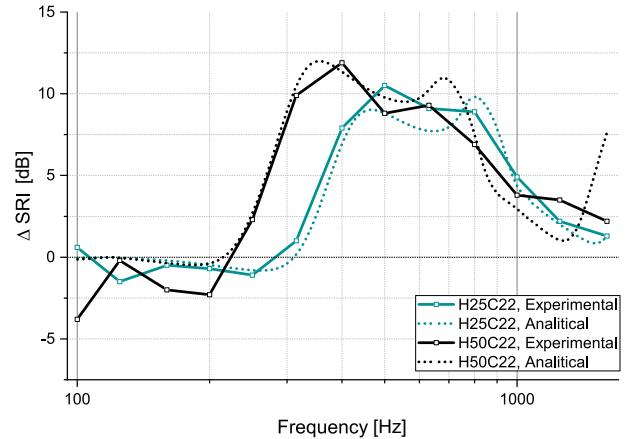


Fig. 11. Gain in sound reduction coefficient due to perforating the honeycomb insertion plate. Solid line – experimental results, dotted line – analytical results calculated with Eq. (4).

#### 4.5. Summarised results

Table 6 recapitulates the main results from the performed tests. The sound insulation and sound absorption parameters are compared along with the surface mass and thickness of the sample.

## 5. Conclusions

This work is a comprehensive study of paper and paper-based products' acoustic parameters, including the absorption, insulation, and dynamic mechanical properties.

Paper and paper-based products prove to be promising substitutes for conventional construction materials, especially concerning the wide manufacture selection on the market. The primary findings are individual for every material type:

- cellulose wool is widely used as a thermal and acoustic insulator by the time mentioned. Its sound absorption coefficient reaches values similar to fibreglass;
- the dynamic mechanical properties of paperboard depend on the machine manufacture direction and frequency. The SRI of the plate with a surface mass of  $2 \text{ kg/m}^2$  equals 13 dB;
- the SRI of multiple layered corrugated cardboard may approach relatively high values. Five layered (10 walls) structure has an SRI of 19 dB–22 dB while maintaining a low surface mass – below  $3 \text{ kg/m}^2$ . The insulation does not differ significantly on the wall type but can be improved, in high frequencies, by gluing the layers;
- the honeycomb panels' structure gives a possibility for easy acoustic parameters enhancement. Perforation produces a grid of Helmholtz resonators, which triggers an increase in the sound

absorption coefficient. When placed in a double-panel, the construction becomes Acoustic Meta-material with a negative bulk modulus, which results in SRI shift up to 6 dB. Such structures have insulation comparable to that of over three times heavier, single 12.5 mm plasterboard (27 dB (ŁĄTKA *et al.*, 2022)).

### Acknowledgments

This research was supported by the National Centre for Research and Development of Poland (the grant number Lider/60/0250/L-11/19/NCBR/2020).

The author Jerzy F. Łątka was supported by the Polish National Agency for Academic Exchange under the Bekker NAWA Programme (the grant number PPN/BEK/2018/1/00383).

The authors thank the KFB Acoustics for providing with the laboratory equipment, necessary to conduct reliable tests.

### References

1. ABD RASHID A.F., YUSOFF S. (2015), A review of life cycle assessment method for building industry, *Renewable and Sustainable Energy Reviews*, **45**: 244–248, doi: [10.1016/j.rser.2015.01.043](https://doi.org/10.1016/j.rser.2015.01.043).
2. ARENAS J.P., REBOLLEDO J., DEL REY R., ALBA J. (2014), Sound absorption properties of unbleached cellulose loose-fill insulation material, *BioResources*, **9**(4): 6227–6240, doi: [10.15376/biores.9.4.6227-6240](https://doi.org/10.15376/biores.9.4.6227-6240).
3. ASDRUBALI F., PISELLO A.L., D’ALESSANDRO F., BIANCHI F., CORNICCHIA M., FABIANI C. (2015), Innovative cardboard based panels with recycled materials from the packaging industry: Thermal and acoustic performance analysis, *Energy Procedia*, **78**: 321–326, doi: [10.1016/j.egypro.2015.11.652](https://doi.org/10.1016/j.egypro.2015.11.652).
4. ASTM E756-05 (2005), *Standard test method for measuring vibration-damping properties of materials*, ASTM Standards (Reapproved 2017).
5. ASTM E2611-19 (2019), *Standard test method for normal incidence determination of porous material acoustical properties based on the transfer matrix method*, ATM International.
6. CRIPPS A. (2004), Cardboard as a construction material: A case study, *Building Research & Information*, **32**(3): 207–219, doi: [10.1080/09613210410001686273](https://doi.org/10.1080/09613210410001686273).
7. COX T.J., D’ANTONIO P. (2016), *Acoustic Absorbers and Diffusers: Theory, Design and Application*, 3rd ed., pp. 91–131, Spon Press.
8. DIARTE J., SHAFFER M. (2021), Cardboard architecture. Eight decades of exploration in academic research and professional practice 1940–2019, *Enquiry The ARCC Journal for Architectural Research*, **18**(1): 17–40, doi: [10.17831/enqarcc.v18i1.1103](https://doi.org/10.17831/enqarcc.v18i1.1103).
9. International Organization for Standardization (2000), Acoustics. Measurement of sound insulation in buildings and of building elements using sound intensity. Part 1: Laboratory measurements, (ISO Standard No. 15186-1:2000), <https://www.iso.org/standard/26097.html>.
10. JASIOLEK A., NOSZCZYK P., ŁĄTKA J.F. (2023), Paper-based building envelopes – Thermal and environmental properties of original envelope designs, *Energy and Buildings*, **289**: 113062, doi: [10.1016/j.enbuild.2023.113062](https://doi.org/10.1016/j.enbuild.2023.113062).
11. KANG C.-W., KIM M.K., JANG E.-S. (2021), An experimental study on the performance of corrugated cardboard as a sustainable sound-absorbing and insulating material, *Sustainability*, **13**(10): 5546, doi: [10.3390/su13105546](https://doi.org/10.3390/su13105546).
12. KLEMM D., HEUBLEIN B., FINK H.P., BOHN A. (2005), Cellulose: Fascinating biopolymer and sustainable raw material, *Angewandte Chemie – International Edition*, **44**(22): 3358–3393, doi: [10.1002/anie.200460587](https://doi.org/10.1002/anie.200460587).
13. KNAACK U., BACH R., SCHABEL S. [Eds.] (2023), *Building with Paper Architecture and Construction*, Birkhäuser.
14. LANGFELDT F., HOPPEN H., GLEINE W. (2020), Broadband low-frequency sound transmission loss improvement of double walls with Helmholtz resonators, *Journal of Sound and Vibration*, **476**: 115309, doi: [10.1016/j.jsv.2020.115309](https://doi.org/10.1016/j.jsv.2020.115309).
15. LATKA J.F. (2017a), House of Cards – design and implementation of a paper house prototype, [in:] *Interfaces: Architecture. Engineering. Science*, pp. 1–10.
16. LATKA J.F. (2017b), *Paper in Architecture: Research by Design, Engineering and Prototyping*, A+BE | Architecture and the Built Environment.
17. ŁĄTKA J.F. *et al.* (2022), Properties of paper-based products as a building material in architecture – An interdisciplinary review, *Journal of Building Engineering*, **50**: 104135, doi: [10.1016/j.jobee.2022.104135](https://doi.org/10.1016/j.jobee.2022.104135).
18. MIYAKE R., LUNA I., GOULD L.A. [Eds.] (2009), *Shigeru Ban: Paper in Architecture*, Rizzoli International Publications.
19. NERI M., LEVI E., CUERVA E., PARDO-BOSCH F., ZABALETA A.G., PUJADAS P. (2021), Sound absorbing and insulating low-cost panels from end-of-life household materials for the development of vulnerable contexts in circular economy perspective, *Applied Sciences*, **11**(12): 5372, doi: [10.3390/app11125372](https://doi.org/10.3390/app11125372).
20. NISKANEN K. [Ed.] (2011), *Mechanics of Paper Products*, De Gruyter, doi: [10.1515/9783110254631](https://doi.org/10.1515/9783110254631).

21. RICCIARDI P., BELLONI E., COTANA F. (2014), Innovative panels with recycled materials: Thermal and acoustic performance and Life Cycle Assessment, *Applied Energy*, **134**: 150–162, doi: [10.1016/j.apenergy.2014.07.112](https://doi.org/10.1016/j.apenergy.2014.07.112).
22. SCHÖNWÄLDER J., ROTS J.G. (2008), Mechanical behaviour of cardboard in construction, *Cardboard in Architecture*, **7**: 131, doi: [10.3233/978-1-58603-820-5-131](https://doi.org/10.3233/978-1-58603-820-5-131).
23. SECCHI S., ASDRUBALI F., CELLAI G., NANNIPIERI E., ROTILI A., VANNUCCHI I. (2016), Experimental and environmental analysis of new sound-absorbing and insulating elements in recycled cardboard, *Journal of Building Engineering*, **5**: 1–12, doi: [10.1016/j.jobee.2015.10.005](https://doi.org/10.1016/j.jobee.2015.10.005).
24. WANG Y., JIANG Z., LI L., QI Y., SUN J., JIANG Z. (2023), A bibliometric and content review of carbon emission analysis for building construction, *Buildings*, **13**(1): 1–22, doi: [10.3390/buildings13010205](https://doi.org/10.3390/buildings13010205).
25. WOLF A., REBECCA B., NIHAT K., KNAACK U., WILFINGER M. (2021), A full performance paper house, *Journal of Facade Design and Engineering*, **9**(1): 117–130, doi: [10.7480/jfde.2021.1.5533](https://doi.org/10.7480/jfde.2021.1.5533).
26. ZABALZA BRIBIÁN I., VALERO CAPILLA A., ARANDA USÓN A. (2011), Life cycle assessment of building materials: Comparative analysis of energy and environmental impacts and evaluation of the eco-efficiency improvement potential, *Building and Environment*, **46**(5): 1133–1140, doi: [10.1016/j.buildenv.2010.12.002](https://doi.org/10.1016/j.buildenv.2010.12.002).